Dalton Transactions

ROYAL SOCIETY OF CHEMISTRY

PAPER

View Article Online
View Journal | View Issue

Cite this: *Dalton Trans.*, 2022, **51**, 5175

What controls the magnetic anisotropy in heptacoordinate high-spin cobalt(II) complexes? A theoretical perspective†

Peter Comba, *[a] Gopalan Rajaraman, *[b] Arup Sarkar[b] and Gunasekaran Velmurugan[a]

Received 18th November 2021,
Accepted 4th March 2022

DOI: 10.1039/d1dt03903b

rsc.li/dalton

The magnetic anisotropy of sixteen seven-coordinate high-spin Co^{II} complexes with O, N, Cl and I donors was investigated with state-of-the-art *ab initio* CASSCF/NEVPT2 calculations and compared with experimental data. Based on the nature of the equatorial and axial ligands, which were found to tune the zero-field splitting, the complexes were classified into four groups. The experimental zero-field splitting parameters D which, for the various structures are in a range of +30 to +60 cm^{-1}, as well as the g and E values are well reproduced. The investigation of the electronic structure shows that in these pentagonal bipyramidal complexes the donors and symmetry in the equatorial plane play an important role in the values of the axial zero-field splitting parameter D, and breaking of the horizontal plane of symmetry was found to enhance the magnitude of the D value. Although negative values of D are a desired condition for SIMs, many Co^{II} based SIMs with positive zero-field splitting are fundamentally important to understand the nature of magnetic anisotropy, and seven coordinate Co^{II} complexes with a large overall crystal field splitting might provide a way forward in this class of molecules.

Introduction

Single molecule magnets (SMM) have been known for a long time. The first, an Mn_{12} complex, synthesized and structurally characterized in 1980 and characterized in 1993, displays slow relaxation of magnetization and hysteresis below the blocking temperature T_B.[1,2] After the unique properties of Mn_{12} were recognized, a great interest in SMMs arose. As the name suggests, the central feature of an SMM is that, unlike classical magnets, their magnetism has a purely molecular origin.[3] Below the blocking temperature, the reorientation of the magnetization is completely blocked due to the magnetization reversal barrier known as U_{eff}. For transition metal SMMs this picture corresponds to the energy separation between the $\pm M_s$ levels. The fact that the M_s states split is due to zero-field splitting (ZFS), which plays a central role for SMMs. The zero-field splitting depends on first order spin–orbit coupling for lanthanides and on second order spin–orbit coupling for transition metal systems.[4] Reasons for the great interest in SMMs are possible applications in the fields of molecular spintronics,[5] high density data storage,[2] and quantum information processing.[6–10] As in Mn_{12}, SMMs can consist of several metal ions connected by ligands, and an SMM with only one metal center is a single ion magnet (SIM). The first SIM was published in 2003 and had a lanthanide ion in its center, and the first transition metal ion containing SIM was a cobalt(II) compound reported in 2011.[11–13]

Important advantages of transition metal based SIMs are that these are generally air-stable, relatively easy to prepare and control of the magnetic anisotropy may be achieved by fine-tuning of the ligand field *via* systematic changes of the ligands.[13,14] The best reported 3d transition metal ion containing SIMs have $Fe^{II/III}$, Co^{II} or Ni^{II} centers.[15–19] However, out of these metals, Co^{II} is the favored candidate due to its Kramers nature of the spin ground state. A vast number of Co^{II} SIMs with coordination numbers of 2 to 7 have been prepared and characterized.[20] For pentagonal bypyramidal (pbp or pseudo-pbp) seven-coordinate Co^{II} SIMS, the equatorial plane is often occupied by a linear or macrocyclic pentadentate ligand.

For a systematic synthesis of complexes for applications as SIMs, it is desirable to be able to accurately correlate the magnetic properties with the molecular structure. Therefore, the computation of electronic structure-based properties, which all depend on the structure, may help to interpret experimental magnetic data. Ligand field theory shows that the multiplet splitting strongly depends on the d-orbital energies, which

[a]*Heidelberg University, Institute of Inorganic Chemistry and Interdisciplinary Center for Scientific Computing, Im Neuenheimer Feld 270, 69120 Heidelberg, Germany. E-mail: peter.comba@aci.uni-heidelberg.de*
[b]*Department of Chemistry, Indian Institute of Technology Bombay, Powai, Mumbai, 400076, India. E-mail: rajaraman@chem.iitb.ac.in*

†Electronic supplementary information (ESI) available. See DOI: 10.1039/d1dt03903b

determine spin–orbit coupling and magnetic anisotropy in these types SIM.[19,21] While four- and six-coordinate Co^{II} complexes are common and well covered in published theoretical and experimental work, theoretical studies on seven-coordinate Co^{II} complexes[22,23] are scarce.[22,23] Here, we present an analysis of sixteen seven-coordinate Co^{II} complexes with pseudo-D_{5h} symmetry, based on *ab initio* CASSCF/NEVPT2 methods to estimate the D and E/D values, in order to understand how various factors such as symmetry, donor atoms, structural distortions and rigidity of the ligand can influence the zero-field splitting.

Computational details

The experimental structures of the Co^{II} complexes shown in Fig. 1 are published, and the coordinates of the isolated molecular cations were used for the computational work. The CASSCF-NEVPT2 calculations were performed with ORCA 4.0.1.[24] Hydrogen atom positions of the X-ray structures were optimized prior to single-point *ab initio* calculations using the UKS/BP86 method with a def2-SVP basis set. The guess orbitals for the multi-configuration self-consistent field methods were generated with a fast ROKS/BP86 setup, involving the BP86 functional and the ZORA-def2-SVP basis set. The ZORA-def2-TZVP basis set was used for cobalt to better describe the metal center, while ZORA-def2-TZVP(-f) was used for the atoms of the first coordination sphere. These basis sets were retained for the CASSCF and NEVPT2 calculations. However, the auxiliary basis sets have been changed from SARC/J to def2-TZVP/C and for the metal center and its environment to def2-SVP/C, respectively. To calculate the excited state energies of the high-spin d^7 Co^{II} system, five 3d-orbitals were used primarily as the active space in the CASSCF calculation. The effect of the second d-shell (4d orbitals) were included with a CAS (7,10) active space in order to account better for electron correlation. In the spin–orbit coupling step, 10 quartet and 40 doublet states, were allowed to mix using the quasi-degenerate perturbation theory (QDPT) treatment as implemented in ORCA. The final ZFS parameters were estimated using the effective Hamiltonian approach.[25] Additionally, the Shape 2.1 program[26] was used to systematically assign the geometries of the seven-coordinate Co^{II} geometries, and the PHI program[27] served to validate the theoretically obtained ZFS parameters and g-factors with experimentally determined parameters from the susceptibility and magnetization data of complexes (**13**) and (**15**).

Results and discussion

The sixteen seven-coordinate Co^{II} complexes studied here are shown in Fig. 1 (structural drawings appear in the ESI, Scheme S1†). The SHAPE analysis (ESI, Table S1†) indicates that the geometries are best described as pseudo-pentagonal bipyramidal. With respect to the ligand systems used, the structures are divided into four classes (see Table 1 and Fig. 1). Class I complexes (**1–3**) have two bidentate nitrates in the equatorial plane and three meridionally disposed pyridine-derived monodentate ligands. Class II complexes (**4–7**) are coordinated to an N_2O_3 macrocyclic ligand in the equatorial plane with two pendant nitrogen donors as axial ligands, and complexes **4–6** only differ in terms of the crystal lattice, *i.e.*, by the non-coordinating counter anions. Class III complexes (**8** and **9**) have the same in-plane N_5-macrocyclic ligand and differ by the axial donors. Class IV complexes (**10–16**) have a linear pentadentate equatorial N_3O_2 ligand with differing protonation states of the hydrazine groups and various axial ligands.

The CASSCF/NEVPT2 method has been shown to accurately estimate spin-Hamiltonian parameters of mononuclear transition metal complexes.[23,35,39–52] The computed ZFS parameters of all 16 complexes considered here are assembled in Table 1 together with a structural parameter describing the in-plane deviation from PBP symmetry and published experimental and computed ZFS parameters. To evaluate the accuracy of the theoretical methodology applied here, the experimental DC magnetic susceptibility and magnetization plots were simulated with the computed values: the DC SQUID data of complexes **1**,[28] **2**,[29] **3**,[29] **13**,[37] and **16**[38] were simulated with NEVPT2 computed parameters (see ESI, Fig. S1 and S2†), leading to good agreement with the experimental data. Note that, in general, experimental ZFS parameters are obtained by fitting the magnetic data, and the sign and magnitude of the resulting parameters are not expected to be accurate. Also, it is known that single-determinant DFT methods are not reliable in computing the magnetic properties of anisotropic Co^{II} systems.[53] Therefore, multi-configurational *ab initio* methods were used for simulating the experimental data. Furthermore, we have also expanded the active space to CAS(7,10) with the inclusion of the second d-shell of Co^{II} to understand its effect on the ZFS parameters (see Table S2 in ESI†). We note that the D parameters alter within a margin of ±2 cm^{-1} and E/D with a margin of ±0.01 upon expanding the active space. We report the AILFT orbital energies and discuss the ZFS parameters in the following on the basis of the CAS(7,5)SCF/NEVPT2 calculation results.

There are few reports on the theoretical aspects of the origin of ZFS in seven-coordinate Co^{II} systems,[22,23] and our present study aims at an in-depth understanding of the electronic states as a guide to estimate the ZFS parameters from a first principles approach. The relevant free ion electronic states of $3d^7$ are the quartet ground states ^4F and ^4P, and the doublet states ^2H, ^2G, ^2F, ^2D_a, ^2D_b, and ^2P (see Fig. 2, where only the quartet states are considered). The splitting of the d-orbitals in the distorted pentagonal bipyramidal structures (pseudo-D_{5h}) leads to $(d_{xz}, d_{yz}) < (d_{x^2-y^2}, d_{xy}) < d_{z^2}$ (see Fig. 3 and Table S3†). In class I, three Co^{II} complexes are coordinated by four nitrate O donors and an aromatic nitrogen donor in the equatorial plane with two aromatic nitrogen donors as axial ligands. Due to the asymmetrical binding of NO_3^- with different Co–O bond lengths, complex **2** shows a large splitting

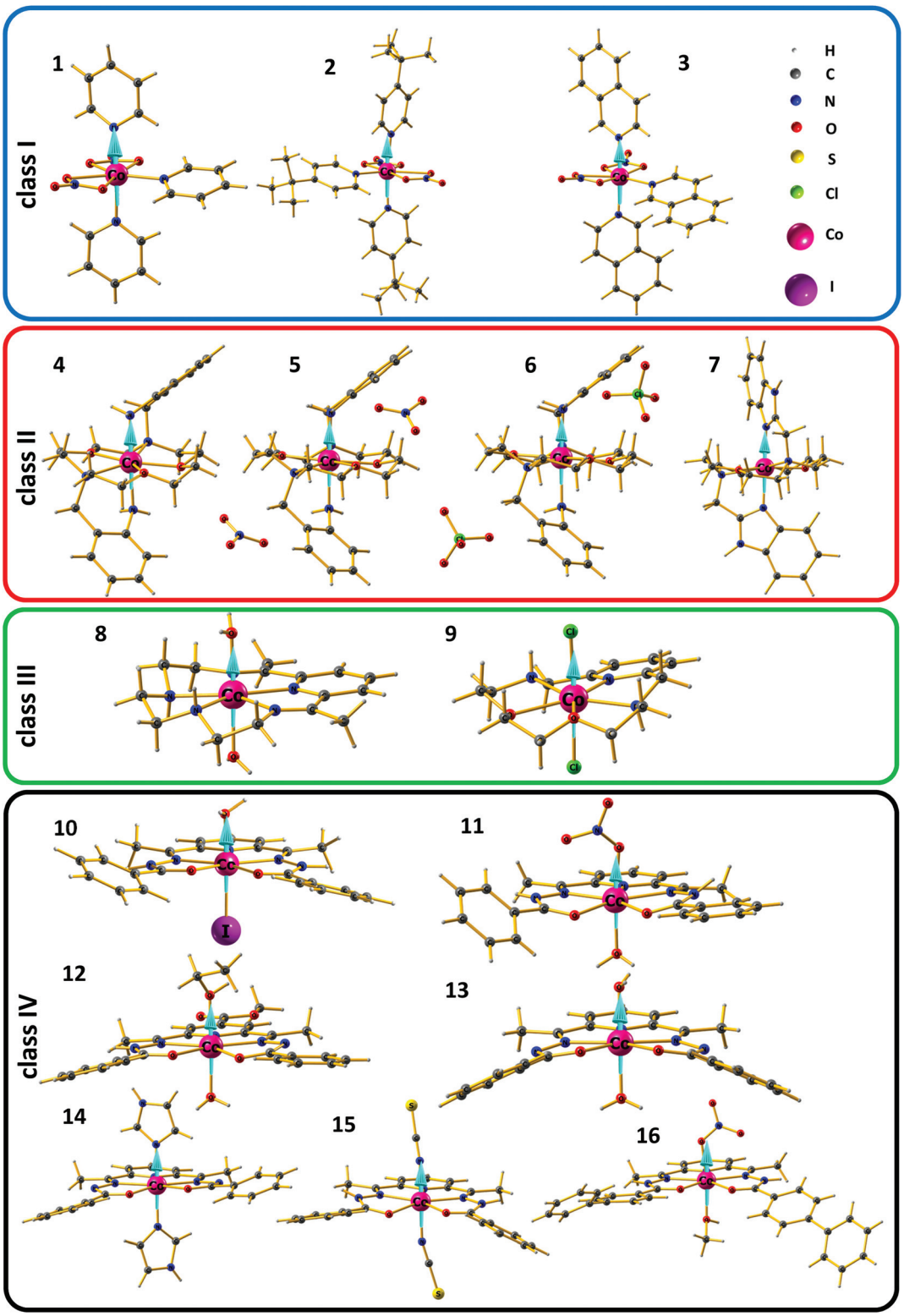

Fig. 1 Structural plots of the chosen heptacoordinate high-spin Co^{II} complexes (structural formula are given in the ESI†); arrows are the computed D_{zz} axis (NEVPT2). Class I: blue box, class II: red box, class III: green box and class IV: black box.

between the equatorial $d_{x^2-y^2}$ and d_{xy} orbitals accompanied by a high E/D value. The SHAPE analysis (see ESI, Table S1†)[54] does not point to this difference within class I complexes and, as expected from the donor sets, the observed splitting is therefore primarily an electronic effect. Furthermore, the complexes also differ in the equatorial coordination patterns. In

Table 1 Comparison of calculated and experimental zero-field splitting parameters of the seven-coordinate mononuclear Co^{II} complexes

	Complexes	Angular distortion parameter (δ °)[a]	NEVPT2 level of theory		Earlier work exp. (calc.) values		Ref.
			D cm^{-1}	E/D	D cm^{-1}	E/D	
Class I	$[Co(py)_3(NO_3)_2]$ (**1**)	68.4	40.78	0.07	68.7 (36)[b]	0.07	28
	$[Co(tbp)_3(NO_3)_2]$ (**2**)	70.1	61.74	0.26	35.8	0.00	29
	$[Co(isq)_3(NO_3)_2]$ (**3**)	66.0	40.83	0.12	35.7	0.00	29
Class II	$[Co(L_1)]^{2+}$ (**4**)	11.7	31.34	0.14	—	—	30
	$[Co(L_1)]\cdot 2NO_3$ (**5**)	11.8	31.35	0.14	25	0	30
	$[Co(L_1)]\cdot 2ClO_4$ (**6**)	11.8	31.34	0.14	26	0	30
	$[Co(L_2)]^{2+}$ (**7**)	14.5	30.49	0.12	23.1	—	31
Class III	$[Co(L_3)(H_2O)_2]^{2+}$ (**8**)	7.3	35.15	0.02	24.6	0	32
	$[Co(L_4)Cl_2]$ (**9**)	7.4	47.30	0.04	40 (45)[c]	0	33
Class IV	$[Co(L_5H_2)I(H_2O)]I$ (**10**)	5.6	36.97	0.03	30	0.01	34
	$[Co(L_5H_2)(H_2O)(NO_3)]$ (**11**)	12.9	35.50	0.07	31 (35)[c]	0 (0.02)[c]	35
	$[Co(L_5H)(H_2O)(EtOH)]^{+}$(**12**)	11.2	37.51	0.00	27.65	0	36
	$[Co(L_5)(H_2O)]$ (**13**)	14.8	34.37	0.06	13.1 (12)[d]	0	37
	$[Co(L_5)(im)_2]$ (**14**)	19.1	35.00	0.06	24.8	0	32
	$[Co(L_5H_2)(NCS)_2]$ (**15**)	10.6	38.07	0.05	15.9 (15)[d]	0	37
	$[Co(NO_3)(EtOH)]^{+}$ (**16**)	11.0	38.21	0.01	33.4	0	38

[a] $\delta = \sum |72 - A_i^{eq}|$, *i.e.*, averaged distortion of the equatorial donor-metal-donor angles from the ideal 72°. [b] CASSCF/RASSI-SO method. [c] SA-CASSCF/NEVPT2 method. [d] Coupled perturbed DFT method.

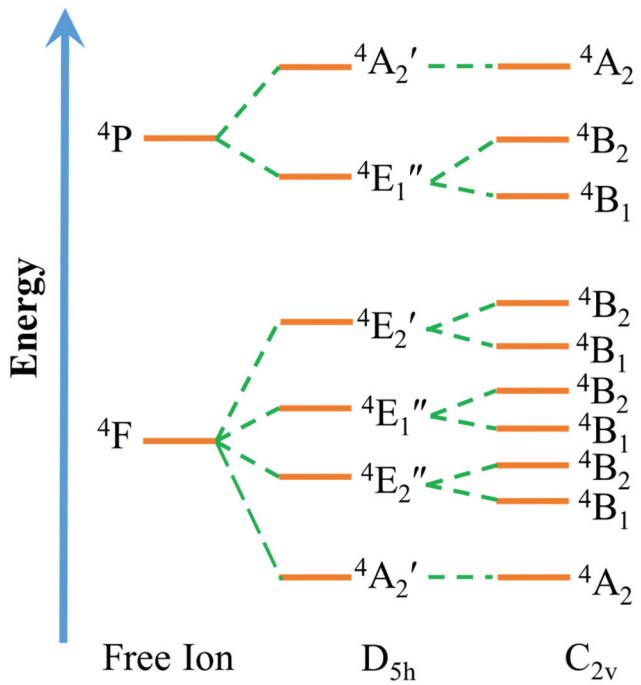

Fig. 2 Qualitative energy splitting diagram of Co^{II}, with sequential perturbations due to the ligand field, free ion → D_{5h} → C_{2v}. The lowering of symmetry allows mixing of the wavefunction, contributing to the D value.

order to quantify this difference, we have introduced the angular distortion parameter δ (see Table 1), which is a measure of the sum over the equatorial bond angle deviations (A^{eq}) from the ideal 72° in PBP geometry, given by $\delta = \sum_i |72 - A_i^{eq}|$. This parameter helps to understand the deviation of the equatorial symmetry from ideal PBP geometry and hence correlates with the ZFS parameters.[17,55] However, since not all equatorial donor atoms are in a plane, the δ parameter does not fully account for the deviation from ideal PBP geometry. Therefore, the one electron ligand field d-orbital energies given in Fig. 3 (see also ESI, Table S2†) are important to rationalize the origin of the magnetic anisotropy.

The ligand field analysis indicates that the first four excited states predominantly contribute to the overall D value (see Fig. 4 and 5). In all four classes, the ground state electronic configuration is approx., *i.e.*, to >80%, $d_{xz^2}{}^2 d_{yz^2}{}^2 d_{x^2-y^2}{}^1 d_{xy}{}^1 d_{z^2}{}^1$. In perfect D_{5h} point group symmetry, this non-degenerate ground state transforms as $^4A_2'$. Excitation of a single electron from d_{yz}/d_{xz} to the $d_{xy}/d_{x^2-y^2}$ orbital set will give rise to the two doubly degenerate excited states $^4E_1''$ and $^4E_2''$ (in D_{5h}, *i.e.*, if there is a horizontal symmetry plane), as shown in Fig. 2. There will be another doubly degenerate $^4E_2'$ state arising from the ^4F term, which lies higher in energy and contributes negligibly to the ZFS. From these two doubly degenerate excited states only $^4E_1''$ contributes significantly to the overall D value in the 16 complexes considered here (see ESI, Tables S4–S51†). The $^4E_2''$ and $^4E_2'$ states do not significantly contribute to the D and E values because the $\hat{L}_x$ and $\hat{L}_y$ operators, transforming as E_1'' in D_{5h}, can only connect the ground state $^4A_2'$ to the $^4E_1''$ excited state with a non-zero matrix element, *i.e.*, $\langle {}^4A_2' | l_{x,y} | {}^4E_1'' \rangle \neq 0$. Due to the mixing of the first four excited states, arising from different spin allowed electronic transitions ($d_{xz}/d_{yz} \rightarrow d_{xy}/d_{x^2-y^2}$), the D value in all D_{5h} or pseudo-D_{5h} complexes are positive. When the symmetry is lowered from $D_{5h} \rightarrow C_{2v}$, the doubly degenerate states $^4E_1''$ and $^4E_2''$ split into four $^4B_1$ and $^4B_2$ states, allowing further mixing with $^4A_2'$ *via* the angular momentum operators. Hence, the complexes with symmetry lower than D_{5h} or pseudo-D_{5h} show contributions from all four excited states. An increase of the structural in-plane distortion described by δ leads to a lowering in sym-

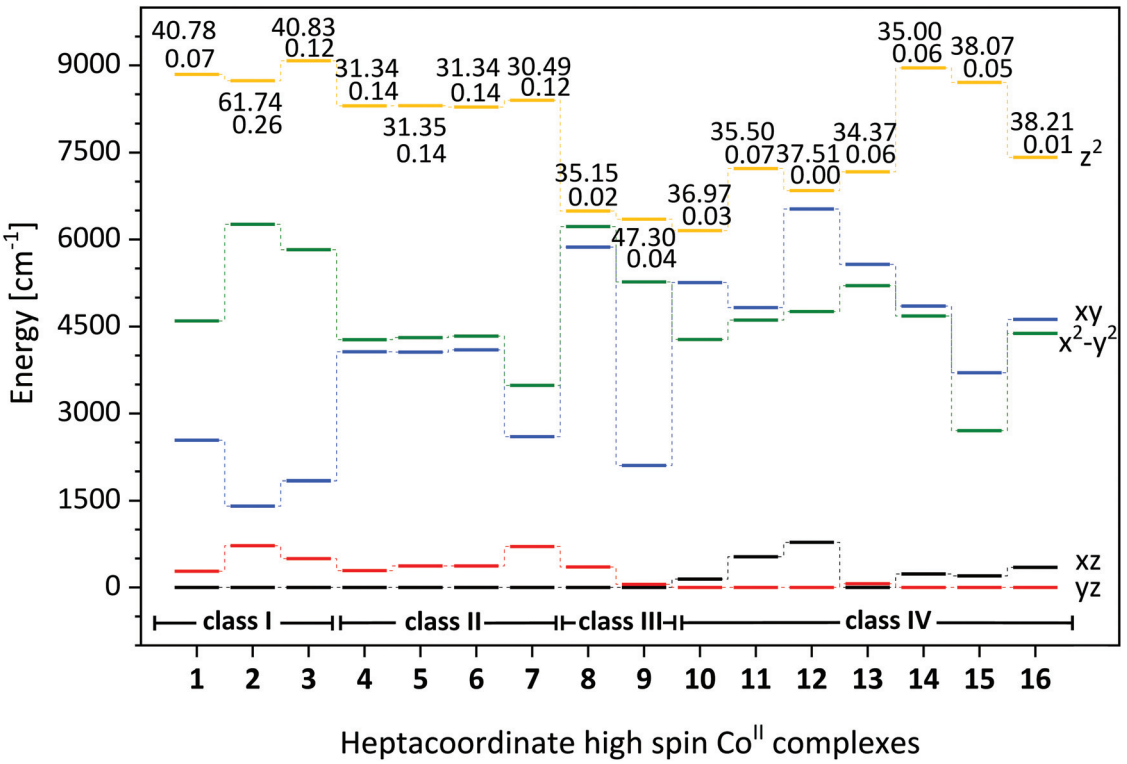

Fig. 3 NEVPT2 computed ligand field d-orbital splitting diagram of the investigated complexes with their respective *D* (top, in cm^{-1}) and *E*/*D*-values (bottom).

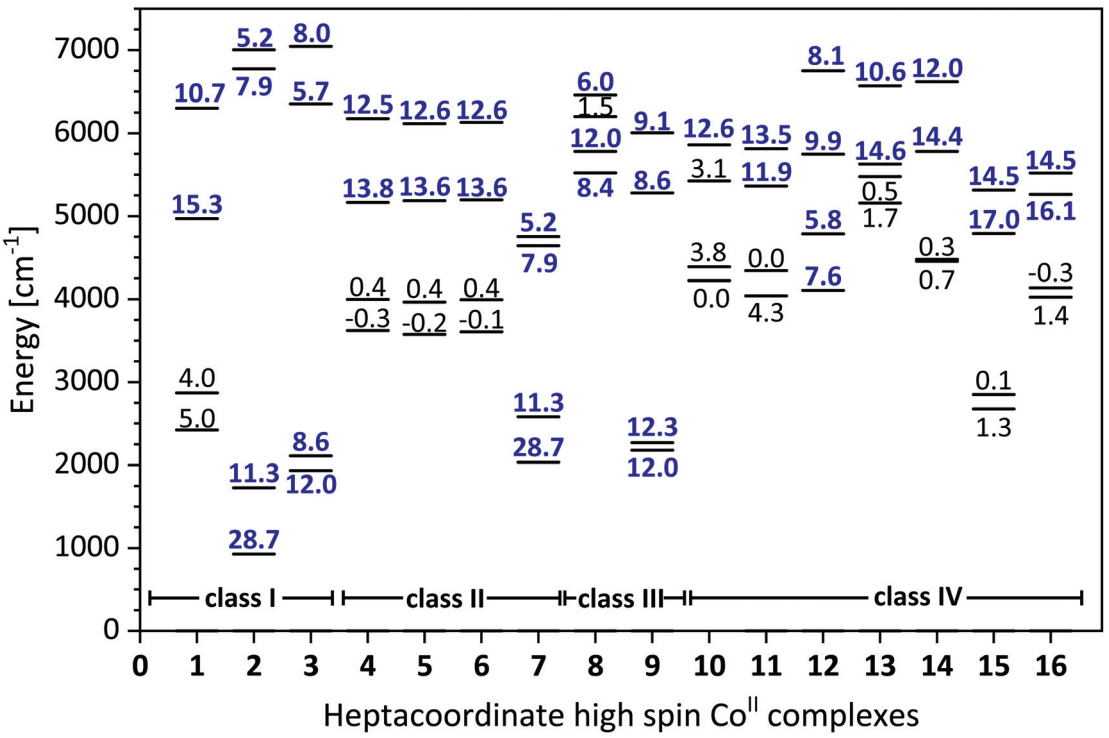

Fig. 4 Contribution of the first four excited states to the *D* parameters for the sixteen Co^{II} complexes.

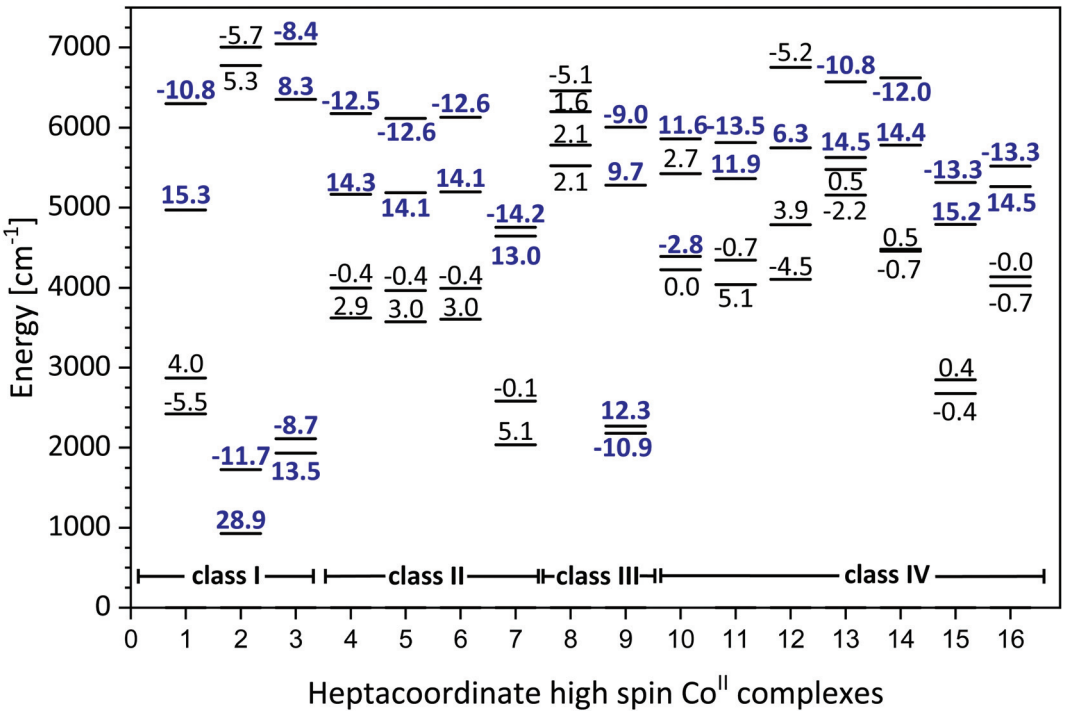

Fig. 5 Contribution of the first four excited states to the *E* parameters for the sixteen Co^{II} complexes.

metry and hence allows further mixing with the excited states. Other higher-lying excited states involving double excitations do not contribute to the zero-field splitting. Also, the $d_{xz}/d_{yz} \rightarrow d_{z^2}$ transitions are too high in energy to significantly contribute to the *D* values. A non-negligible positive contribution towards *D* arises from a spin-flipped excited state involving the $d_{xy} \rightarrow d_{x^2-y^2}$ transition and corresponds to the $^2A_1'$ representation. This contribution rises in the cases, where these two orbitals remain close in energy.

The NEVPT2/QDPT/EHA computed spin-Hamiltonian parameters are compared with the experimental data in Table 1 (see also ESI, Tables S4–S51†), and a comparison of experimental with simulated χT *vs.* *T* data of three complexes is given in the ESI (Fig. S1 and S2†). The *ab initio* computed major anisotropy axes, *i.e.*, D_{zz} and g_{zz} are aligned along the highest order axis (C_5) in all complexes (see ESI, Fig. S3–S17†). The axial ligands control the energy of the d_{z^2} orbital to a large extent; due to strong axial coordination, the energy of the d_{z^2} orbitals in all these complexes remains above the $d_{x^2-y^2}/d_{xy}$ set of orbitals and hence the $d_{xz}/d_{yz} \rightarrow d_{z^2}$ transitions prevail at high energy. It follows that the equatorial ligands primarily determine the contribution arising from lower energy excited states and therefore control the major spin-allowed part of the ZFS parameters. The angular distortion parameter δ shows the highest deviation (>60°) in all three class I complexes, and this helps to break the equatorial ligand field symmetry. Therefore, class I complexes show the highest axial ZFS parameters with *D* values ranging from +40 cm^{-1} in complex **1** to +62 cm^{-1} in complex **2**. The SHAPE analysis (see Table S1 in ESI†) also reveals the largest deviation parameter for PBPY symmetry for complexes **1–3**.

Experimental EPR data are available for complexes **1** and **3**.[28,29] In complex **1** the *g*-factors derived from EPR spectra for the ground state Kramers doublets (KDs) are $g_1 = 6.1$, $g_2 = 4.2$ and $g_3 = 2.2$, compared to $g_1 = 5.31$, $g_2 = 4.15$ and $g_3 = 1.97$ obtained from NEVPT2 calculations. From the fitting of χT *vs.* *T* data, a similar *D* value of 35 cm^{-1} for both complexes has been reported,[29] and a downward shift of χT *vs.* *T* is observed at higher temperatures for complex **2** in comparison to **3**, and this supports a higher *D* value for **2** compared to **3**. Therefore, we have simulated both curves with the *ab initio* calculated values, and excellent agreement with the experimental curves was obtained (see ESI, Fig. S2†). This shows that the *ab initio* methods used here can accurately estimate the magnetic anisotropy of these complexes. The three equatorial ligands – two nitrates and a pyridine derivative – break the molecular symmetry from pseudo-D_{5h} to pseudo-C_{2v}. Therefore, all four excited states contribute to the overall *D* values for complexes **2** and **3**. Complex **2** has the weakest ligand field, and the first excited state lies at 920 cm^{-1} (see Fig. 4), leading to the largest value of *D* in the class I series of complexes. The *E* parameter arises from the difference of the D_{xx} and D_{yy} values and, since a high in-plane symmetry reduces the difference between the two values, *E* and the usually reported *E*/*D* parameters are larger for complex **2** than for the other complexes **1** and **3** (see Table 1 and Fig. 5 and 6).

Due to the equatorial coordination of a pentadentate macrocyclic ligand in class II, complexes **4** to **7** possess little distortion from D_{5h} symmetry and the δ parameter is only approx. 12°. Therefore, the main contribution to *D* arises from $^4E_1''$, *i.e.*, from the 3rd and 4th excited state. As therefore

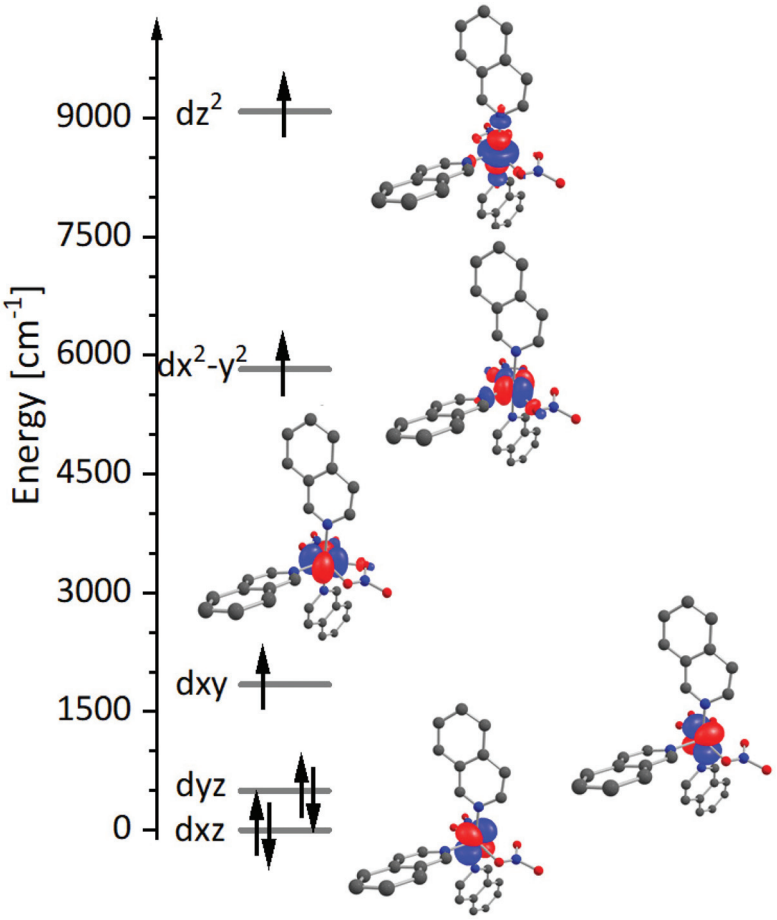

Fig. 6 AILFT orbital energy diagram for $[Co(isq)_3(NO_3)_2]$ (complex **3**).

expected, the computed D values are smaller than those of class I, and primarily this is due to the higher in-plane ligand field exerted by the macrocyclic ligand. As the counter ion does not significantly influence the structure, their influence on the D values is minimal, and the D values of the class II compounds remain in the range of 30–32 cm^{-1} with moderate E/D values around 0.12.

The two class III complexes **8** and **9** are coordinated to a pentadentate macrocyclic ligand with two monodentate axial ligands (H_2O, Cl^-). For **8**, there is only little distortion from pseudo D_{5h} symmetry but with an in-plane N_3O_2 donor set in **9**, the in-plane distortions are significant, breaking the D_{5h} symmetry. This is not reproduced by the δ parameter, which for complex **9** is only ~7°. This is because δ is a structural parameter that does not describe the electronics of the metal-donor interaction and also because deviations from planarity of the in-plane ligand field is not included. Therefore, a quantitative (*ab initio*) ligand field calculation is a better way to analyze the d-orbital energies. The monodentate axial ligands lead to a higher symmetry in comparison to the class II systems but to a significant drop of energies of the d_{z^2} orbitals due to a weaker ligand field (see also Fig. 3 and Fig. S9, S10†). Due to the weaker in-plane oxygen donors and the deviation from planarity, complex **9** has much closer excited states than complex **8**. For this reason, complex **9** has a higher D value (+47 cm^{-1}) than **8** (+35 cm^{-1}).

Complexes **10–16** in class IV have a planar open-chain N_3O_2 ligand derived from diacetylpyridine-bis-(benzoyl-hydrazine) (DAPBH) with different protonation states of the hydrazine groups coordinated in the xy plane and various axial ligands. Due to the planar geometry of the pentadentate ligand, the symmetry of the complexes is close to pseudo-D_{5h}. The D values are all around 37 ± 3 cm^{-1}. This supports the assumption that the equatorial donors determine the ZFS parameters of pentagonal bipyramidal Co^{II} complexes. Due to a high equatorial symmetry in class IV complexes, the contribution to D arises from the third and fourth excited states (*i.e.*, from the $^4E_1''$ states). The δ parameters of these complexes vary in an unpredictable way and range from a low 6° in complex **10** to a moderate 19° in complex **14**. Due to the higher symmetry and reduced energy gap between $d_{x^2-y^2}$ and d_{xy} orbitals, the contribution towards D arising from the doublet states is quite large in all class IV complexes. In some cases, the variation of the axial ligands allows breaking the symmetry in the xy plane (complexes **10–12** and **16**). An interesting observation in this class is that, despite the heavier halide (iodide) coordination in the case of complex **10**,

this is not enhance the D parameter, which again highlights the dominant role of structural parameters in determining the sign and magnitude of D in transition metal SIMs. The DC magnetic data of complexes **13** and **14** are simulated with the *ab initio* electronic parameters in excellent agreement with the experimentally observed data (see Fig. S2†).

The E/D parameter for the complexes in classes III and IV range from 0.01 to 0.07. This is one order of magnitude smaller than for the other two classes and is due to the cancellation of transverse anisotropic values (D_{xx} and D_{yy}). The D_{xx} and D_{yy} values arise from the spin–orbit coupling of excited states with different M_L values. If the equatorial ligands enforce a higher symmetry, these two terms cancel each other, leading to the small rhombic magnetic anisotropies in complexes **10–16** (see Fig. 5).

Conclusions

The CASSCF/NEVPT2 computational approach with a CAS(7,5) active space yields D and E/D values that are in excellent agreement with available experimental data. With respect to the ligands coordinated to Co^{II}, we have divided the sixteen pentagonal bipyramidal complexes into four classes. In contrast to other geometries, the ZFS parameters of the seven-coordinate Co^{II} complexes are all rather similar, with D always positive and in the range of 30–60 cm^{-1}. The magnitudes of D and E/D are rationalized on the basis of the equatorial angle distortion parameter δ and the *ab initio* computed d-orbital energies. For all four classes of complexes, the major contribution to the D value arises from the mixing of the first four excited states. Among the four classes studied, class I shows the largest magnitude of D due to a large splitting of the $^4E_2''$ term. This arises from the relatively weak equatorial ligand field and structural distortions that cause a reduction in the pseudo D_{5h} symmetry. Complex **2** shows the highest D value of 61 cm^{-1} due to a significant deviation from the equatorial 5-fold symmetry with a large δ parameter. The detailed analysis reveals that the ZFS of these pseudo-pentagonal-bipyramidal Co^{II} complexes strongly depends on the nature of equatorial ligands and related distortions that lower the symmetry. Therefore, out-of-plane symmetry breaking and weaker equatorial coordination is the key to enhance the ZFS in Co^{II}-based seven coordinate SIMs. Future work in this area might be extended with the aim to further change the equatorial ligand symmetry, further tune the D parameter and eventually change its sign.

Conflicts of interest

There are no conflicts to declare.

Acknowledgements

This work was conducted within the Max Planck School Matter to Life, supported by the German Federal Ministry of Education and Research (BMBF) in collaboration with the Max Planck Society. We also acknowledge support by Heidelberg University, the German Research Foundation (DFG) and the state of Baden-Württemberg for computer resources on bwHPC. GR would like to thank DST and SERB (CRG/2018/00430; DST/CSA-03/2018-10; SB/SJF/2019-20/12) for funding and AS for an IPDF fellowship by IIT Bombay.

References

1 T. Lis, *Acta Crystallogr., Sect. B: Struct. Crystallogr. Cryst. Chem.*, 1980, **36**, 2042–2046.
2 R. Sessoli, D. Gatteschi, A. Caneschi and M. Novak, *Nature*, 1993, **365**, 141.
3 J. M. Frost, K. L. Harriman and M. Murugesu, *Chem. Sci.*, 2016, **7**, 2470–2491.
4 M. Nanomagnets, in *Structure and Bonding*, ed. S. Gao, Springer-Verlag, Berlin-Heidelberg, 2015, vol. 164.
5 L. Bogani and W. Wernsdorfer, in *Nanoscience And Technology: A Collection of Reviews from Nature Journals*, World Scientific, 2010, pp. 194–201.
6 A. Furrer and O. Waldmann, *Rev. Mod. Phys.*, 2013, **85**, 367.
7 D. Gatteschi and R. Sessoli, *Angew. Chem., Int. Ed.*, 2003, **42**, 268–297.
8 E. M. Chudnovsky and J. Tejada, *Macroscopic quantum tunneling of the magnetic moment*, Cambridge University Press, 2005.
9 M. Dressel, B. Gorshunov, K. Rajagopal, S. Vongtragool and A. Mukhin, *Phys. Rev. B: Condens. Matter Mater. Phys.*, 2003, **67**, 060405.
10 J. Van Slageren, S. Vongtragool, B. Gorshunov, A. Mukhin, N. Karl, J. Krzystek, J. Telser, A. Müller, C. Sangregorio and D. Gatteschi, *Phys. Chem. Chem. Phys.*, 2003, **5**, 3837–3843.
11 N. Ishikawa, M. Sugita, T. Ishikawa, S.-y. Koshihara and Y. Kaizu, *J. Am. Chem. Soc.*, 2003, **125**, 8694–8695.
12 J. M. Zadrozny and J. R. Long, *J. Am. Chem. Soc.*, 2011, **133**, 20732–20734.
13 T. Jurca, A. Farghal, P.-H. Lin, I. Korobkov, M. Murugesu and D. S. Richeson, *J. Am. Chem. Soc.*, 2011, **133**, 15814–15817.
14 M. Murrie, *Chem. Soc. Rev.*, 2010, **39**, 1986–1995.
15 J. M. Zadrozny, D. J. Xiao, M. Atanasov, G. J. Long, F. Grandjean, F. Neese and J. R. Long, *Nat. Chem.*, 2013, **5**, 577–581.
16 X.-N. Yao, J.-Z. Du, Y.-Q. Zhang, X.-B. Leng, M.-W. Yang, S.-D. Jiang, Z.-X. Wang, Z.-W. Ouyang, L. Deng and B.-W. Wang, *J. Am. Chem. Soc.*, 2016, **139**, 373–380.
17 G. A. Craig, A. Sarkar, C. H. Woodall, M. A. Hay, K. E. Marriott, K. V. Kamenev, S. A. Moggach, E. K. Brechin, S. Parsons and G. Rajaraman, *Chem. Sci.*, 2018, **9**, 1551–1559.
18 P. C. Bunting, M. Atanasov, E. Damgaard-Møller, M. Perfetti, I. Crassee, M. Orlita, J. Overgaard, J. Van Slageren, F. Neese and J. R. Long, *Science*, 2018, **362**, eaat7319.

19 A. Sarkar, S. Dey and G. Rajaraman, *Chem. – Eur. J.*, 2020, **26**, 14036–14058.
20 A. K. Bar, C. Pichon and J.-P. Sutter, *Coord. Chem. Rev.*, 2016, **308**, 346–380.
21 S. Gomez-Coca, E. Cremades, N. Aliaga-Alcalde and E. Ruiz, *J. Am. Chem. Soc.*, 2013, **135**, 7010–7018.
22 A. K. Mondal, A. Mondal, B. Dey and S. Konar, *Inorg. Chem.*, 2018, **57**, 9999–10008.
23 D. Darmanović, I. N. Shcherbakov, C. Duboc, V. Spasojević, D. Hanžel, K. Anđelković, D. a. Radanović, I. Turel, M. Milenković and M. Gruden, *J. Phys. Chem. C*, 2019, **123**, 31142–31155.
24 F. Neese, *Wiley Interdiscip. Rev.: Comput. Mol. Sci.*, 2018, **8**, e1327.
25 R. Maurice, R. Bastardis, C. d. Graaf, N. Suaud, T. Mallah and N. Guihery, *J. Chem. Theory Comput.*, 2009, **5**, 2977–2984.
26 M. C. Llunell, D. Casanova , J. Cirera, P. Alemany and S. Alvarez, *S.SHAPE, version 2.1*, Universitat de Barcelona, Barcelona, 2013.
27 N. F. Chilton, R. P. Anderson, L. D. Turner, A. Soncini and K. S. Murray, *J. Comput. Chem.*, 2013, **34**, 1164–1175.
28 E. Bartolomé, P. J. Alonso, A. Arauzo, J. Luzón, J. Bartolomé, C. Racles and C. Turta, *Dalton Trans.*, 2012, **41**, 10382–10389.
29 L. Chen, S.-Y. Chen, Y.-C. Sun, Y.-M. Guo, L. Yu, X.-T. Chen, Z. Wang, Z. Ouyang, Y. Song and Z.-L. Xue, *Dalton Trans.*, 2015, **44**, 11482–11490.
30 C. Platas-Iglesias, L. Vaiana, D. Esteban-Gómez, F. Avecilla, J. A. Real, A. de Blas and T. Rodríguez-Blas, *Inorg. Chem.*, 2005, **44**, 9704–9713.
31 L. Vaiana, M. Regueiro-Figueroa, M. Mato-Iglesias, C. Platas-Iglesias, D. Esteban-Gómez, A. de Blas and T. Rodríguez-Blas, *Inorg. Chem.*, 2007, **46**, 8271–8282.
32 X.-C. Huang, C. Zhou, D. Shao and X.-Y. Wang, *Inorg. Chem.*, 2014, **53**, 12671–12673.
33 B. Drahos, R. Herchel and Z. Travnicek, *Inorg. Chem.*, 2015, **54**, 3352–3369.
34 L. J. Batchelor, M. Sangalli, R. g. Guillot, N. Guihéry, R. Maurice, F. Tuna and T. Mallah, *Inorg. Chem.*, 2011, **50**, 12045–12052.
35 R. Ruamps, L. J. Batchelor, R. Maurice, N. Gogoi, P. Jiménez-Lozano, N. Guihéry, C. de Graaf, A. L. Barra, J. P. Sutter and T. Mallah, *Chem. – Eur. J.*, 2013, **19**, 950–956.
36 F. Schleife, A. Rodenstein, R. Kirmse and B. Kersting, *Inorg. Chim. Acta*, 2011, **374**, 521–527.
37 M. Dey, S. Dutta, B. Sarma, R. C. Deka and N. Gogoi, *Chem. Commun.*, 2016, **52**, 753–756.
38 A. K. Bar, N. Gogoi, C. Pichon, V. D. P. Goli, M. Thlijeni, C. Duhayon, N. Suaud, N. Guihéry, A. L. Barra and S. Ramasesha, *Chem. – Eur. J.*, 2017, **23**, 4380–4396.
39 S. Vaidya, A. Upadhyay, S. K. Singh, T. Gupta, S. Tewary, S. K. Langley, J. P. Walsh, K. S. Murray, G. Rajaraman and M. Shanmugam, *Chem. Commun.*, 2015, **51**, 3739–3742.
40 S. Vaidya, S. K. Singh, P. Shukla, K. Ansari, G. Rajaraman and M. Shanmugam, *Chem. – Eur. J.*, 2017, **23**, 9546–9559.
41 K. Chattopadhyay, M. J. H. Ojea, A. Sarkar, M. Murrie, G. Rajaraman and D. Ray, *Inorg. Chem.*, 2018, **57**, 13176–13187.
42 S. Vaidya, P. Shukla, S. Tripathi, E. Rivière, T. Mallah, G. Rajaraman and M. Shanmugam, *Inorg. Chem.*, 2018, **57**, 3371–3386.
43 S. Tripathi, S. Vaidya, K. U. Ansari, N. Ahmed, E. Riviere, L. Spillecke, C. Koo, R. d. Klingeler, T. Mallah and G. Rajaraman, *Inorg. Chem.*, 2019, **58**, 9085–9100.
44 X.-N. Yao, M.-W. Yang, J. Xiong, J.-J. Liu, C. Gao, Y.-S. Meng, S.-D. Jiang, B.-W. Wang and S. Gao, *Inorg. Chem. Front.*, 2017, **4**, 701–705.
45 E. A. Suturina, D. Maganas, E. Bill, M. Atanasov and F. Neese, *Inorg. Chem.*, 2015, **54**, 9948–9961.
46 A. K. Mondal, M. Sundararajan and S. Konar, *Dalton Trans.*, 2018, **47**, 3745–3754.
47 M. S. Fataftah, S. C. Coste, B. Vlaisavljevich, J. M. Zadrozny and D. E. Freedman, *Chem. Sci.*, 2016, **7**, 6160–6166.
48 Y. Rechkemmer, F. D. Breitgoff, M. Van Der Meer, M. Atanasov, M. Hakl, M. Orlita, P. Neugebauer, F. Neese, B. Sarkar and J. Van Slageren, *Nat. Commun.*, 2016, **7**, 1–8.
49 L. J. Batchelor, M. Sangalli, R. Guillot, N. Guihéry, R. Maurice, F. Tuna and T. Mallah, *Inorg. Chem.*, 2011, **50**, 12045–12052.
50 A. Sarkar, S. Tewary, S. Sinkar and G. Rajaraman, *Chem. – Asian J.*, 2019, **14**, 4696–4704.
51 J. Acharya, A. Sarkar, P. Kumar, V. Kumar, J. F. Gonzalez, O. Cador, F. Pointillart, G. Rajaraman and V. Chandrasekhar, *Dalton Trans.*, 2020, **49**, 4785–4796.
52 M. A. Hay, A. Sarkar, G. A. Craig, L. Bhaskaran, J. Nehrkorn, M. Ozerov, K. E. R. Marriott, C. Wilson, G. Rajaraman, S. Hill and M. Murrie, *Chem. Sci.*, 2019, **10**, 6354–6361.
53 M. Atanasov, D. Aravena, E. Suturina, E. Bill, D. Maganas and F. Neese, *Coord. Chem. Rev.*, 2015, **289–290**, 177–214.
54 M. Llunell, D. Casanova, J. Cirera, P. Alemany and S. Alvarez, *SHAPE, version 2.1*, Universitat de Barcelona, Barcelona, Spain, 2013.
55 A. Sarkar, R. Jose, H. Ghosh and G. Rajaraman, *Inorg. Chem.*, 2021, **60**(13), 9680–9687.